Materials Today Communications 39 (2024) 108809

Contents lists available at ScienceDirect

Materials Today Communications

journal homepage: www.elsevier.com/locate/mtcomm

Remarkable strengthening of nanolayered metallic composites by nanoscale crystalline interfacial layers

Yaodong Wang [a,b,1], Kaiqing Dai [a,b,1], Wenjun Lu [c], Shaohua Chen [d], Jianjun Li [a,b,*]

[a] College of Mechanical and Electrical Engineering, Central South University, Changsha 410083, Hunan, PR China
[b] State Key Laboratory of Precision Manufacturing for Extreme Service Performance, Central South University, Changsha 410083, Hunan, PR China
[c] Department of Mechanical and Energy Engineering, Southern University of Science and Technology, Shenzhen 518055, PR China
[d] Institute of Advanced Structure Technology, Beijing Institute of Technology, Beijing 100081, PR China

ARTICLE INFO

Keywords:
Strength
Interfaces
Crystalline interfacial layers
Dislocation nucleation

ABSTRACT

Strengthening of metallic materials has been a long-standing scientific issue. Recent experiments have shown that the introducing of nanoscale amorphous interfacial layers is capable of providing effective strengthening in metallic materials. However, the above strategy is subject to the complexity of the composition and structure in the amorphous layers that usually contains at least two elements with significant concentration variation along the interfacial thickness. Here in this paper it is demonstrated by experiments that significant strengthening can be achieved in a Cu/Ni nanolayered metallic composite by architecting nanoscale single-elemental crystalline (instead of amorphous) interfacial layers into the layered interfacial region. The results show that the hardness of the composite with individual layer thickness of 40 nm exhibits a first-increase-and-then-decrease trend with the decreasing of the thickness of the crystalline (aluminum as an example) interfacial layer from 40 to 2 nm, leading to a maximum value of 5.67 GPa, which is around 22% higher than that of the normal sample without the interfacial layers (4.66 GPa). Further molecular dynamics simulations revealed that the strength enhancement originated from the increase in the lattice mismatch of the layered interfaces due to the addition of crystalline interfacial layers. The interfaces with larger lattice mismatch possess more dense dislocation networks, which relieves the stress concentration at interfaces. Hence, dislocations are much harder to nucleate, resulting in a substantial strengthening in the nanolayered composite. As a result, this work provides a simple effective strengthening strategy by inserting nanoscale crystalline interfacial layers to increase the lattice mismatch of nanolayered interfaces.

1. Introduction

Designing stronger metallic materials is a long-standing pursuit of scientists in materials science and engineering. To achieve this purpose, many strategies have been developed to strengthen metallic materials and composites, one of which is reducing their intrinsic structure size (e.g., grain size [1–3], twin thickness [4], or layer thickness [5,6]) into the nanoscale. For example, Youssef et al. [7] synthesized nanocrystalline copper with a tensile yield strength of 791 MPa by means of milling, the strength of which is about one order of magnitude higher than that of conventional coarse-grained copper. The ultra-high strength is attributed to the restricted dislocation motions induced by their small grain size of 23 nm. Another typical example is that a nano-twinned copper fabricated by Lu et al. [8] through pulsed electrodeposition obtained a tensile yield strength of as high as 900 MPa by reducing the twin thickness to 15 nm.

The size-refinement strategy has also been employed in the nanolayered composites [9–13]. For instance, Nizolek et al. [14] designed a Cu/Nb nanolayered composite with yield strength as high as 1056 MPa by reducing the individual layer thickness down to 15 nm through an accumulative roll bonding technique. Similarly, an ultra-strong Nb/a--CuNb nanolayered composite with a hardness of 8.57 GPa is obtained by Qin et al. [15] through reducing the individual layer thickness to 5 nm using direct current magnetron sputtering. Also, Zhang et al. [16]

* Correspondence to: College of Mechanical and Electrical Engineering, and State Key Laboratory of Precision Manufacturing for Extreme Service Performance, Central South University, Changsha, 410083, Hunan, PR China.
E-mail addresses: mejjli@csu.edu.cn, jianjunli.mech@hotmail.com (J. Li).
[1] These authors contribute equally to this work.

https://doi.org/10.1016/j.mtcomm.2024.108809
Received 30 January 2024; Received in revised form 2 February 2024; Accepted 1 April 2024
Available online 3 April 2024

discovered that the yield strength of Cu/Zr nanolayered composites as prepared by direct current magnetron sputtering can reach as high as 2750 MPa by decreasing the individual layer thickness to 5 nm.

However, the strengthening of metallic materials by intrinsic size effect has approached a limit due to the inverse Hall-Petch relation that originates from the transition from dislocation-dominated deformation to grain boundary (or phase interface) mediated one due to the confined space in nanograins [17–21]. Hence, the strength of the nanostructured metallic materials is still far less than the theoretical value (~G/10) [22]. Another disadvantage of the size refinement strategy is that the strengthening is gained at the expense of the tensile ductility and plasticity [23–29]. The limited plasticity is attributed to strain localization behavior, a typical form of which is the shear band [30–33].

Recently, experiments have shown that the introduction of nanoscale interfacial layers has been approved to be an effective route to strengthen metallic materials without losing their tensile ductility and plasticity [34–38]. For example, Khalajhedayati et al. [39] prepared a Cu-Zr alloy that contains nanograins of 30 nm in diameter and amorphous intergranular films by segregating dopants. The newly designed alloy shows a yield strength of 1086 MPa, which is 326 MPa larger than that of nanocrystalline Cu with the same grain size. The enhanced yield strength is attributed to the reduction in grain boundary energy induced by interfacial segregation, which restrains dislocation nucleation [40, 41]. Another example is that Wu et al. [42] obtained a highly deformable nanostructured Mg alloy with a near-ideal strength of 3.6 GPa by constructing a supra-nanometer-sized dual-phase glass-crystal structure, i.e., $MgCu_2$ nanograins of around 6 nm are surrounded by 2 nm thick amorphous interfacial films. Most recently, using arc melting and thermomechanical processing, Yang et al. [43] synthesized a $Ni_{43.9}Co_{22.4}Fe_{8.8}Al_{10.7}Ti_{11.7}B_{2.5}$ high entropy alloy with an ultrahigh strength of 1.6 GPa and a good tensile ductility of 25% by introducing 5 nm disordered nanoscale interfacial layers among the micrometer-sized ordered superlattice grains.

The above-mentioned nanoscale amorphous interfacial layers usually consist of two or more elements and show a complicated structure [44–48], increasing the difficulty in exploring the strengthening mechanisms, which is unfavorable in providing a simple and effective strengthening strategy. Interestingly, significant strengthening can be achieved by introducing single-element crystalline interfacial layers (CILs) [49–51]. Yan et al., [52] revealed that the nano-hardness of a 5 nm Cu/Ni/W nanolayered composite prepared by magnetron sputtering is more than 9 GPa, which is larger than that of the bi-metallic counterparts, such as Cu/Ni, Cu/W and Cu/Cr. The previous molecular dynamics (MD) simulation of the authors also predicts that a Cu/Ni nanolayered composite can be significantly strengthened by inserting Ag interfacial layers [53]. The addition of Ag interfacial layers increases the lattice mismatch that reduces the stress concentration at the interfaces. Hence, dislocations are much harder to nucleate, resulting in the strengthening effect. However, the simulation results lack an experimental confirmation. It is also interesting to know whether the strategy is universal, i.e., the fcc/fcc nanolayered composites can be strengthened by introducing a single crystalline interfacial layer that can increase the lattice mismatch of interfaces. In addition, establishing a relation between the characteristic parameters of the interface and strength provides a guideline for the design of nanoscale interfacial layers with complex element composition and structures.

Here, aluminium was selected as the crystalline interfacial layers (CILs) of different thicknesses (from 2 to 40 nm) to increase the lattice mismatch of the interfaces in a Cu/Ni nanolayered composite with an individual layer thickness of 40 nm by magnetron sputtering. The experiments have shown that the nano-hardnesses of the composite with Al interfacial layers are much larger than that of the CIL-free counterpart with a nano-hardness of 4.66 GPa. Also, the nano-hardness is highly CIL thickness-dependent, leading to a maximum value of 5.67 GPa at 5 nm. The further MD simulation results demonstrated that the strengthening effect is attributed to the bigger difficulty in dislocation nucleation as generated by the larger lattice mismatch and elastic modulus.

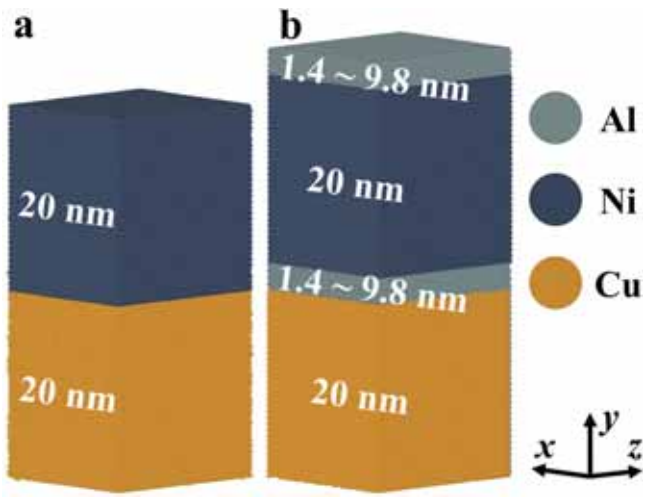

Fig. 1. Initial configurations of the simulated models for the (a) CIL-free sample with individual layer thickness of 20 nm and (b) the CIL samples with different Al layer thicknesses. The thickness of Al interlayers varies from 1.4 nm to 9.8 nm.

2. Methodology

2.1. Experimental details

The 40 nm Cu/Ni nanolayered composites with Al crystalline interfacial layers (CILs) of different thicknesses (h) (called as CIL samples) were deposited on the Si (100) substrate by magnetron sputtering (PTL6S PVD system), where Ni is deposited by radio frequency magnetron sputtering and the other two elements are deposited by direct current one. The h value varies from 2 nm to 40 nm (i.e., h=2, 5, 10, 20 and 40 nm), corresponding to five CIL composites respectively named as CIL-2, CIL-5, CIL-10, CIL-20, and CIL-40 samples. The deposition process was carried out in the order of Cu-Al-Ni-Al, where targets of pure Cu (99.99%), Ni (99.99%) and Al (99.99%) were used. The 40 nm Cu/Ni nanolayered composite without CILs (called as CIL-free sample) was also prepared by alternately stacking Cu and Ni layers for comparison. The base pressure before deposition was less than 8.0×10^{-5} Pa and the Ar pressure was maintained to be 0.3 Pa during deposition. The substrate was rotated at a frequency of 30 rpm to ensure the uniformity of the sample. The deposition rate of Cu, Ni and Al were determined to be 0.2068, 0.0744 and 0.1226 nm/s, respectively. The nominal total thicknesses of the CIL-2, CIL-5, CIL-10, CIL-20, and CIL-40 were designed to be 1.18, 1.17, 1.2, 1.2 and 1.28 μm, respectively. The nominal total thickness of the CIL-free samples is 1.2 μm.

The crystal structure of the CIL-40 sample was studied using X-ray diffraction (XRD, Bruker D8 Advance), and the internal microstructure of the composite was characterized using transmission electron microscopy (TEM, Talos F200X G2) that is equipped with energy dispersive spectroscopy (EDS) detector. All TEM samples were prepared by etching using a focused ion beam (FIB, FEI Helios Nanolab 600i). The hardness test of the samples was conducted by the continuous stiffness method using a Nano-indenter system (Keysight, Agilent G200), with a strain rate of 0.05 s^{-1} during the test. In order to avoid the substrate effect, the maximum depth of indentation was set to be 350 nm, and ten repeated tests were conducted on each sample to ensure the reliability of the data.

2.2. Simulation models

The compression of four Cu/Ni CIL samples with Al layer thicknesses of 1.4, 2.8, 4.9 and 9.8 nm under three loading directions was simulated

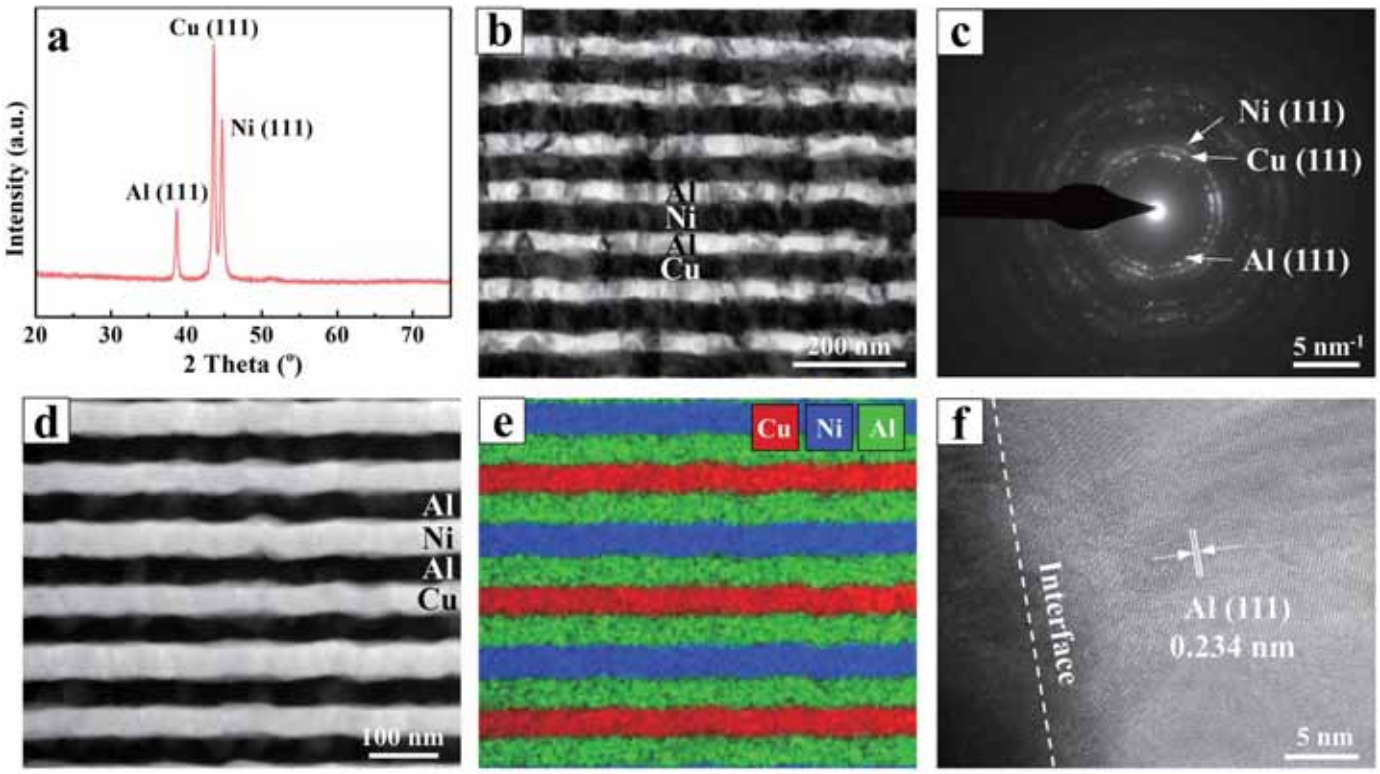

Fig. 2. Microstructural characterization of 40 nm Cu/Ni nanolayered composites with 40 nm Al interfacial layers: (a) XRD pattern; (b) Bright-field TEM image; (c) SAED pattern; (d) HAADF-STEM image; (e) the corresponding EDS map; and (f) HRTEM image of the Al interfacial layer and the adjacent interface.

by molecular dynamics (Fig. 1). The simulations of CIL-free samples were also conducted for comparison. The CIL-free model was constructed by alternately stacking 20 nm Cu and Ni layers (Fig. 1a), while the CIL ones were built by inserting Al layers between the 20 nm Cu and Ni layers (Fig. 1b). All the crystalline layers are single crystals with a crystalline orientation of $x = [11\bar{2}]$, $y = [111]$ and $z = [1\bar{1}0]$, forming (111)/(111) semi-coherent interfaces that are common in fcc/fcc systems [54–56]. The final dimensions of the above four CIL models are $17.3 \times 43.1 \times 19.2\text{nm}^3$, $17.3 \times 45.8 \times 19.2\text{nm}^3$,$17.3 \times 50 \times 19.2\text{nm}^3$ and $17.3 \times 59.8 \times 19.2\text{nm}^3$, respectively. The final dimension of the

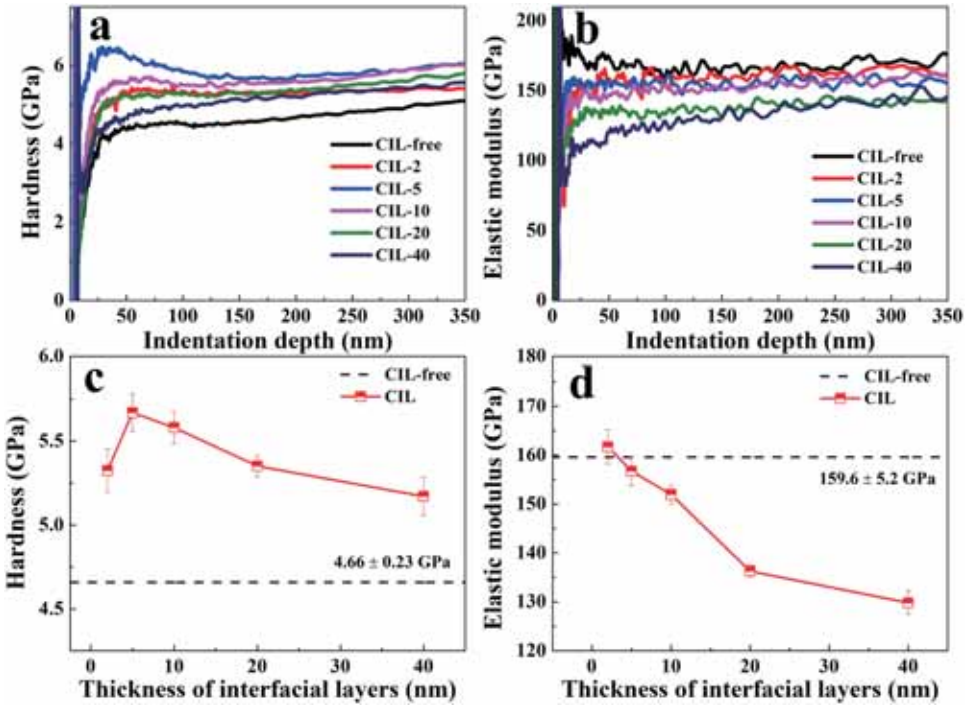

Fig. 3. Representative indentation depth-dependent (a) nano-hardness and (b) elastic modulus of all CIL Cu/Ni samples. The measured Al layer thickness-dependent (c) nano-hardness and (d) elastic modulus of all CIL Cu/Ni samples. Those of the CIL-free sample were also included for comparison.

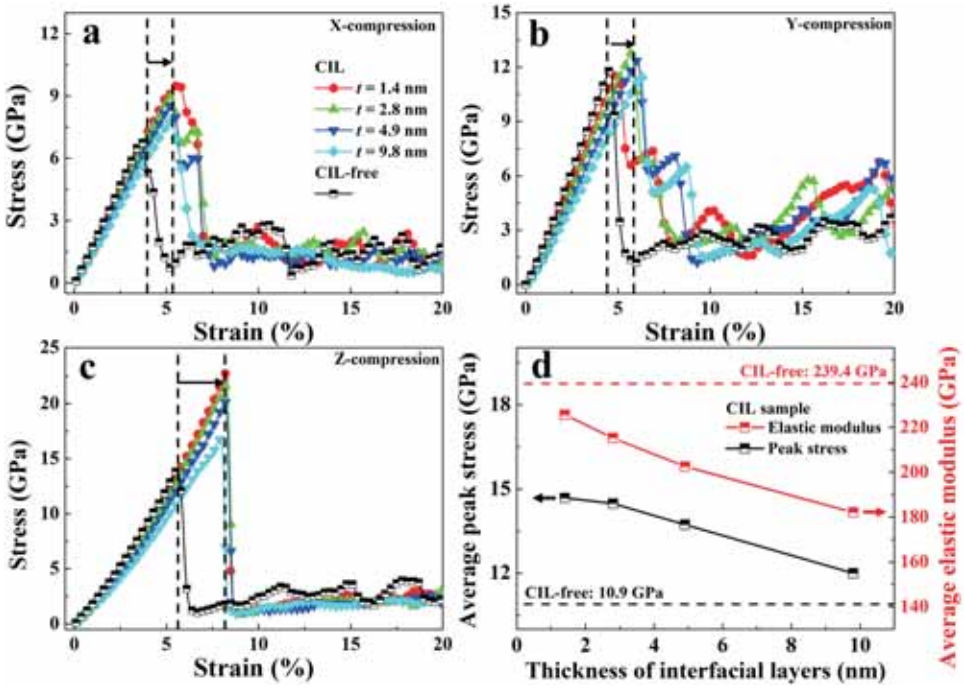

Fig. 4. Simulated stress-strain curves of all CIL samples under (a) *x*-, (b) *y*- and (c) *z*-compression, where *t* is the thickness of interfacial layers in the simulation models. (d) The average peak stresses and elastic modulus of all CIL samples under three loading directions as a function of the thickness of interfacial layers. The corresponding data for the CIL-free sample are also included for comparison.

CIL-free model is nm^3. All these models were built through ATOMSK [57].

All the compression simulations were performed by LAMMPS (Large-scale Atomic/Molecular Massively Parallel Simulator) [58] with periodic boundary conditions in three directions at a time step of 1 fs. The embedded atom method (EAM) potentials used in this study were developed by Zhou et al. [59], which is able to give correct basic material properties such as lattice constants and elastic constants. Before compression, an energy minimization process is employed. Then, under the isothermal-isobaric (NPT), all samples were relaxed for 200 ps with stress-free in three directions at 50 K. Next, the models were compressed at 50 K with a constant strain of 5×10^8 s^{-1} under NPT along *x*, *y*, and *z* directions, respectively. Nose–Hoover thermostat and Nose–Hoover barostat were used to control the temperature and pressure, respectively. The evolution of the microstructures of all samples was visualized and analyzed by OVITO [60].

3. Results and discussion

3.1. Microstructure

Take the CIL-40 sample as an example to show the microstructural characterization, which is presented in Fig. 2. The composite shows a crystal structure as confirmed by the XRD pattern in Fig. 2a, where the three diffraction peaks located at 38.7°, 43.5°, and 44.6° correspond to the Al (111), Cu (111), and Ni (111) crystal planes, respectively. As shown in Fig. 2b, a layered structure and relatively straight interfaces can be observed in the TEM. The actual thickness of the Cu, Ni and Al layers of the CIL-40 sample were measured to be 49.9 ± 2.4, 54.4 ± 1.7 and 37.3 ± 2.7 nm, respectively, resulting in an actual total thickness of 1.43 μm for the sample. The corresponding selected area electron diffraction (SAED) pattern is shown in Fig. 2c, indicating that the sample has strong Cu (111), Al (111), and Ni (111) texture [61], echoing well with the above XRD result. The high-angle annular dark-field (HAADF) images (Fig. 2d) and the EDS image (Fig. 2e) corresponding to the HAADF image further demonstrate that the CIL composite has a unique structure in which the Al layers were added between the Cu and Ni layers. The fcc/fcc nanolayered composites prepared by magnetron sputtering usually show (111)//(111) interfaces, where the (111) planes are parallel to the interfaces [52,62]. This structural characteristic was also found in the present samples, i.e., the high-resolution TEM (HRTEM) image in Fig. 2f shows that the Al (111) plane with an interplanar spacing of 0.234 nm is parallel to the interfaces.

3.2. Interfacial layer thickness-dependent strengthening

Fig. 3a and b presents the nano-hardness and elastic modulus of all CIL Cu/Ni samples as a function of the indentation depth, respectively. The results show that for all samples, the hardness first increases rapidly with increasing indentation depth. Then, the curve reaches a plateau, where hardness remains almost unchanged. The average value of the hardness data in the plateau of the hardness-displacement curves was adopted as the intrinsic hardness of the composites [63]. Here, the intrinsic hardness of all samples was calculated as the average values of hardness in the indentation depth range of 150–200 nm. To avoid the substrate effect, the elastic modulus of the samples was calculated using the data in the range of 100–150 nm, which is ~10 % indentation depth of the total film thickness.

The hardness of the Cu/Ni nanolayered composites with Al interfacial layers as a function of the interfacial layer thickness is shown in Fig. 3c. The result of the CIL-free sample is also shown for comparison. The results show that the nano-hardnesses of all CIL samples are much higher than that of the CIL-free one, and that the harness-CIL thickness relation exhibits a first-increase-then-decrease trend, leading to a maximum one at h=5 nm. Specifically, the CIL-40 sample possesses the smallest hardness (i.e., 5.17 GPa) among all CIL samples. Note that even this smallest value is 10.9% higher than that of the CIL-free one, i.e., 4.66 GPa. The CIL-free and CIL-40 samples have the same constituent layer thickness of 40 nm which results in the same number of interfaces. A difference is the proportion of Al layers, i.e., 0% in the former and 50% in the latter. The difference is not the reason for the increased hardness because the Al layers are much softer than the Cu and Ni layers [56,64].

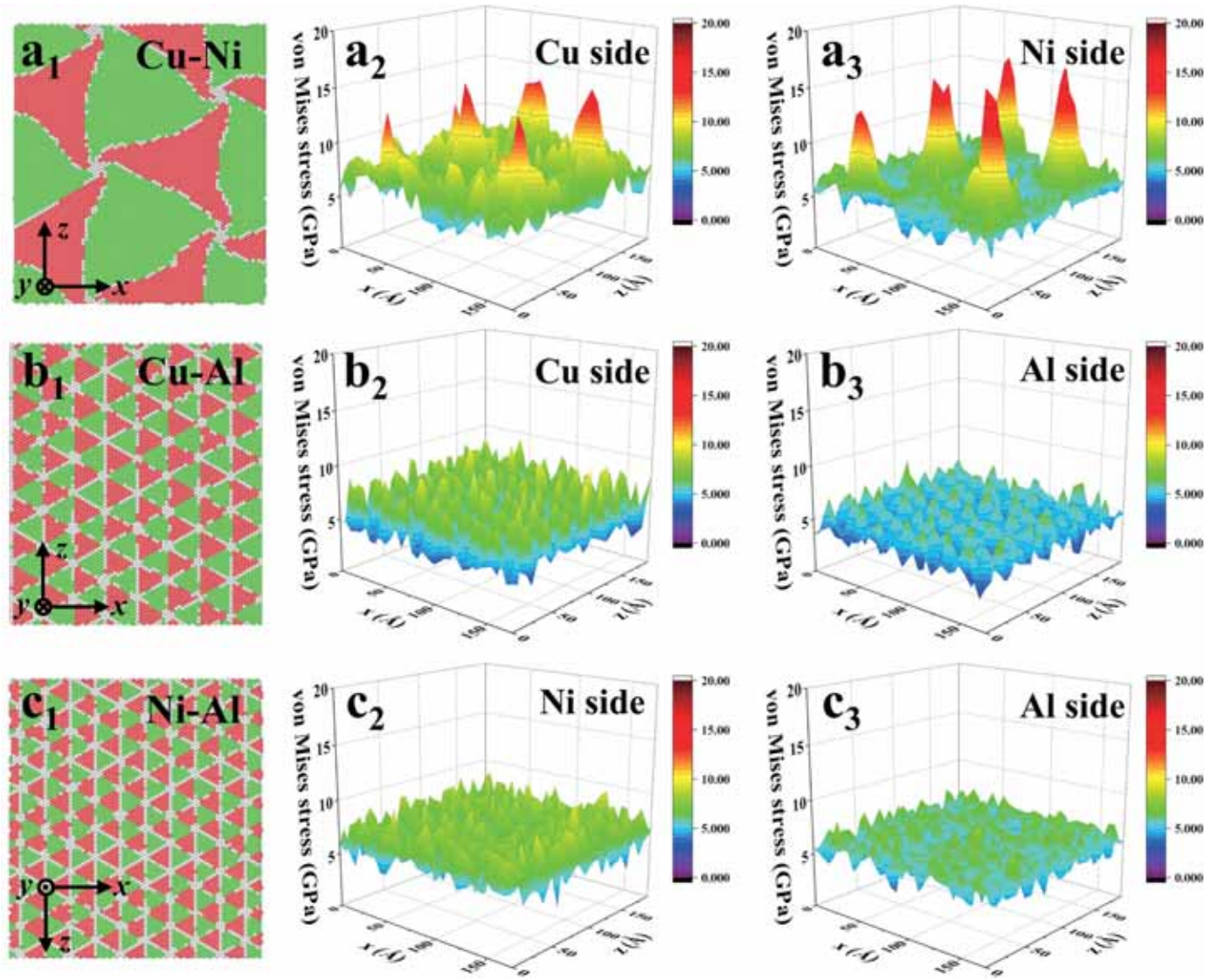

Fig. 5. Microstructures of (a_1) the Cu-Ni interfaces of CIL-free samples, (b_1) the Cu-Al and (c_1) Ni-Al interfaces of the CIL samples with Al interfacial layer of 9.8 nm in simulations. The corresponding distribution of von Mises stress at different sides of the (a_2 and a_3) Cu-Ni, (b_2 and b_3) Cu-Al and (c_2 and c_3) Ni-Al interfaces.

Another difference is that the CIL samples possess Cu-Al and Ni-Al interfaces, instead of the Cu/Ni interfaces in the CIL-free one, which is the main reason for the strengthening behavior and will be explained by the following MD simulation results in the next section. Moreover, the maximum hardness is achieved in the CIL-5 sample, i.e., 5.67 GPa, which is 21.7% higher than that of the CIL-free one. The reduction in hardness as h is smaller than 5 nm might come from the formation of amorphous or the medium-range-order type of structure in the constituent layers deposited by magnetron sputtering [11,65]. Fig. 3d presents the measured elastic modulus of all CIL and CIL-free samples. The results show that the measured elastic modulus of the CIL samples is increased from 129.8 GPa to 161.7 GPa with the decrease of the Al layer thickness from 40 nm to 2 nm, the largest of which is very close to that of the CIL-free sample (i.e., 159.6 GPa) due to the decreased amount of Al phase that possesses smaller elastic modulus than the Cu and Ni ones.

Fig. 4a–c shows the simulated compressive stress-strain responses of all the CIL samples under x, y, and z directions, respectively, where the thickness of the interfacial layers is represented by t. The results of the CIL-free one were also included for comparison. The deformation of these samples can be divided into elastic and plastic stages. Take the CIL-free sample under x-compression as an example (Fig. 4a), the stress increases linearly with increasing strain during the elastic stage. Then, dislocation nucleation occurs at the peak stress, indicating the beginning of the plastic deformation. At the same time, the stress decreases sharply. The addition of Al interfacial layers leads to two variations in the CIL samples. One is the reduction in elastic modulus which is manifested in the reduced slope of the curve during the elastic stage. The other one is the delay of the occurrence of the plastic deformation, which is denoted by the black arrow in Fig. 4a. These phenomena are also observed in the simulations under the other two loading directions (Fig. 4b and c). The addition of Al interfacial layers delays the elastic stage but reduces the elastic modulus, the former behavior shows a strengthening effect and the latter shows a weakening effect. Whether the addition of Al interfacial layers possesses a strengthening effect depends on the competitive relationship between the two behaviors.

The peak stresses under three compression directions of samples were averaged to evaluate the simulated strength of all samples. The average elastic modulus was also calculated based on a similar way. As shown in Fig. 4d, the simulated strength of the CIL samples shows a monotonical increase with respect to the refining Al layers. The simulated maximum and minimum strengthening obtained in the CIL samples can be as high as 34.7% and 10.1% as compared with the CIL-free case. The elastic modulus of CIL samples also increases with decreasing t. The MD simulation results are in good agreement with the

experimental measurements (Fig. 3). A difference is that no softening is observed in the simulations because all the Al interfacial layers were constructed to be crystalline even when it was reduced to be as thin as 1.4 nm.

3.3. The strengthening mechanism in the CIL composites

The strengthening effect in the CIL samples originates from the additional elastic stage, which in turn depends on the dislocation nucleation. To explore the delayed dislocation nucleation in the CIL samples, the simulated microstructures and stress distribution of the Cu-Ni interfaces in the CIL-free sample, and those of the Cu-Al and Ni-Al interfaces in the CIL samples with Al interfacial layers of 9.8 nm-thick are presented in Fig. 5. These fcc/fcc interfaces usually show a triangle dislocation network with a stress concentration on the node [66–68]. The triangle dislocation network is found in the Cu-Ni interfaces in Fig. 5a_1. The von Mises stress distributions of the Cu-Ni interfaces at the Cu and Ni sides are shown in Fig. 5a_2 and a_3, respectively. Several peaks with high values of von Mises stress are observed, which correspond to the positions of dislocation network nodes. The maximum von Mises stress at the Cu and Ni sides are as high as 14.8 and 16.6 GPa, respectively. The density of dislocation is directly proportional to the lattice mismatch. The lattice mismatches of the Cu-Ni, Cu-Al and Ni-Al interfaces are 0.095, 0.435 and 0.53 Å, respectively. Hence, the dislocation density of the Cu-Ni interfaces is the lowest, followed by the Cu-Al interfaces and finally the Ni-Al interfaces (Fig. 5b_1 and c_1). The von Mises stress is still concentrated on the dislocation network nodes at the Cu-Al and Ni-Al interfaces, while the maximum value of the stress is much lower than that in the Cu-Ni interfaces (Fig. 5b_2–c_3). Specifically, the maximum stresses are 11 and 7.6 GPa at the Cu and Al sides of the Cu-Al interfaces, respectively. These values are 9.6 and 8.5 GPa at the Ni and Al sides of the Ni-Al interfaces, respectively. Dislocations are much harder to nucleate in the Cu-Al and Ni-Al interfaces than in the Cu-Ni interfaces because of the reduction in stress concentration. As a result, the CIL samples show a longer elastic stage than the CIL-free samples.

4. Conclusions

In summary, the strengthening of Cu/Ni nanolayered composites has been investigated by nanoindentation tests and MD simulations. The results show that the Cu/Ni nanolayered composites can be strengthened by inserting Al interfacial layers. It is revealed by MD simulations that the stress concentration is much lower in the Cu-Al and Ni-Al interfaces of the samples with Al interfacial layers than in the Cu-Ni interfaces of the CIL-free one, indicating that a larger applied stress is required to activate the plastic deformation in the former than the latter. As a result, the CIL samples are strengthened due to the extension of the elastic stage. The hardness of the CIL samples increases with decreasing interfacial layer thickness from 40 nm to 5 nm, leading to a maximum hardness of 5.67 GPa, which is 1.01 GPa higher than that of the CIL-free one. These findings confirmed that the addition of crystalline interfacial layers that increases the lattice mismatch of interfaces can substantially strengthen the nanolayered metallic composites.

CRediT authorship contribution statement

Yaodong Wang: Investigation, Methodology, Visualization, Formal analysis, Writing – original draft. **Kaiqing Dai**: Investigation, Visualization, Formal analysis, Writing – original draft. **Wenjun Lu**: Writing – review & editing. **Shaohua Chen**: Writing – review & editing. **Jianjun Li**: Conceptualization, Resources, Project administration, Supervision, Funding acquisition, Writing – review & editing.

Declaration of Competing Interest

The authors declare that they have no known competing financial interests or personal relationships that could have appeared to influence the work reported in this paper.

Data availability

Data will be made available on request.

Acknowledgements

This work was supported by the National Natural Science Foundation of China (NSFC) (Grant No. 12272413) and the Department of Science and Technology of Hunan Province (Grant No. 2021RC3022). The support for the computational resources for the atomic simulations from the High-Performance Computing Center of Central South University is appreciated.

References

[1] M.A. Meyers, A. Mishra, D.J. Benson, Mechanical properties of nanocrystalline materials, Prog. Mater. Sci. 51 (2006) 427–556, https://doi.org/10.1016/j.pmatsci.2005.08.003.
[2] M. Dao, L. Lu, R. Asaro, J. Dehosson, E. Ma, Toward a quantitative understanding of mechanical behavior of nanocrystalline metals, Acta Mater. 55 (2007) 4041–4065, https://doi.org/10.1016/j.actamat.2007.01.038.
[3] J. Schiøtz, K.W. Jacobsen, A maximum in the strength of nanocrystalline copper, Science 301 (2003) 1357–1359, https://doi.org/10.1126/science.1086636.
[4] X. Li, Y. Wei, L. Lu, K. Lu, H. Gao, Dislocation nucleation governed softening and maximum strength in nano-twinned metals, Nature 464 (2010) 877–880, https://doi.org/10.1038/nature08929.
[5] A. Misra, J.P. Hirth, R.G. Hoagland, Length-scale-dependent deformation mechanisms in incoherent metallic multilayered composites, Acta Mater. 53 (2005) 4817–4824, https://doi.org/10.1016/j.actamat.2005.06.025.
[6] E.G. Fu, N. Li, A. Misra, R.G. Hoagland, H. Wang, X. Zhang, Mechanical properties of sputtered Cu/V and Al/Nb multilayer films, Mater. Sci. Eng. A 493 (2008) 283–287, https://doi.org/10.1016/j.msea.2007.07.101.
[7] K.M. Youssef, R.O. Scattergood, K.L. Murty, J.A. Horton, C.C. Koch, Ultrahigh strength and high ductility of bulk nanocrystalline copper, Appl. Phys. Lett. 87 (2005) 091904, https://doi.org/10.1063/1.2034122.
[8] L. Lu, X. Chen, X. Huang, K. Lu, Revealing the maximum strength in nanotwinned copper, Science 323 (2009) 607–610, https://doi.org/10.1126/science.1167641.
[9] J.Y. Zhang, S. Lei, J. Niu, Y. Liu, G. Liu, X. Zhang, J. Sun, Intrinsic and extrinsic size effects on deformation in nanolayered Cu/Zr micropillars: from bulk-like to small-volume materials behavior, Acta Mater. 60 (2012) 4054–4064, https://doi.org/10.1016/j.actamat.2012.03.056.
[10] J.Y. Zhang, G. Liu, S.Y. Lei, J.J. Niu, J. Sun, Transition from homogeneous-like to shear-band deformation in nanolayered crystalline Cu/amorphous Cu–Zr micropillars: intrinsic vs. extrinsic size effect, Acta Mater. 60 (2012) 7183–7196, https://doi.org/10.1016/j.actamat.2012.09.027.
[11] Z. Fan, S. Xue, J. Wang, K.Y. Yu, H. Wang, X. Zhang, Unusual size dependent strengthening mechanisms of Cu/amorphous CuNb multilayers, Acta Mater. 120 (2016) 327–336, https://doi.org/10.1016/j.actamat.2016.08.064.
[12] G. Yin, Z. Feng, Z. Zhao, Y. Cao, X. Huang, L. Li, Microstructure and creep properties of Al/Mg/Al composite clad plates, J. Cent. South Univ. 30 (2023) 2867–2877, https://doi.org/10.1007/s11771-023-5437-y.
[13] S. Xu, M. Han, K. Shen, Y. Cao, A. Fu, C. Ding, H. Tang, Fatigue properties of binary Ti-Ta metal-metal composite with lamellar microstructure, J. Cent. South Univ. 30 (2023) 2878–2889, https://doi.org/10.1007/s11771-023-5433-2.
[14] T. Nizolek, I.J. Beyerlein, N.A. Mara, J.T. Avallone, T.M. Pollock, Tensile behavior and flow stress anisotropy of accumulative roll bonded Cu-Nb nanolaminates, Appl. Phys. Lett. 108 (2016) 051903, https://doi.org/10.1063/1.4941043.
[15] F. Qin, F. Chen, J. Hou, W. Lu, S. Chen, J. Li, Strong resistance to shear instability in multilayered metallic composites by nanoscale amorphous-BCC crystalline interfaces, Mater. Sci. Eng. A 891 (2024) 145919, https://doi.org/10.1016/j.msea.2023.145919.
[16] J.Y. Zhang, S. Lei, Y. Liu, J.J. Niu, Y. Chen, G. Liu, X. Zhang, J. Sun, Length scale-dependent deformation behavior of nanolayered Cu/Zr micropillars, Acta Mater. 60 (2012) 1610–1622, https://doi.org/10.1016/j.actamat.2011.12.001.
[17] C.E. Carlton, P.J. Ferreira, What is behind the inverse Hall–Petch effect in nanocrystalline materials? Acta Mater. 55 (2007) 3749–3756, https://doi.org/10.1016/j.actamat.2007.02.021.
[18] A. Giga, Y. Kimoto, Y. Takigawa, K. Higashi, Demonstration of an inverse Hall–Petch relationship in electrodeposited nanocrystalline Ni–W alloys through tensile testing, Scr. Mater. 55 (2006) 143–146, https://doi.org/10.1016/j.scriptamat.2006.03.047.
[19] E.N. Hahn, M.A. Meyers, Grain-size dependent mechanical behavior of nanocrystalline metals, Mater. Sci. Eng. A 646 (2015) 101–134, https://doi.org/10.1016/j.msea.2015.07.075.
[20] S. Takeuchi, The mechanism of the inverse Hall-Petch relation of nanocrystals, Scr. Mater. 44 (2001) 1483–1487, https://doi.org/10.1016/S1359-6462(01)00713-8.

[21] C. Dong, W. Jiang, Molecular dynamics study on the effect of grain size on the plastic deformation of Fe-Cr-Ni alloy nanopolycrystals, Mater. Today Commun. 38 (2024) 107770, https://doi.org/10.1016/j.mtcomm.2023.107770.
[22] G. Wu, S. Balachandran, B. Gault, W. Xia, C. Liu, Z. Rao, Y. Wei, S. Liu, J. Lu, M. Herbig, W. Lu, G. Dehm, Z. Li, D. Raabe, Crystal-glass high-entropy nanocomposites with near theoretical compressive strength and large deformability, Adv. Mater. 32 (2020) 2002619, https://doi.org/10.1002/adma.202002619.
[23] H. Wu, G. Fan, An overview of tailoring strain delocalization for strength-ductility synergy, Prog. Mater. Sci. 113 (2020) 100675, https://doi.org/10.1016/j.pmatsci.2020.100675.
[24] A. Misra, M. Goken, N.A. Mara, I.J. Beyerlein, Hierarchical and heterogeneous multiphase metallic nanomaterials and laminates, MRS Bull. 46 (2021) 236–243, https://doi.org/10.1557/s43577-021-00059-7.
[25] S.D. Antolovich, R.W. Armstrong, Plastic strain localization in metals: origins and consequences, Prog. Mater. Sci. 59 (2014) 1–160, https://doi.org/10.1016/j.pmatsci.2013.06.001.
[26] J. Li, W. Lu, S. Zhang, D. Raabe, Large strain synergetic material deformation enabled by hybrid nanolayer architectures, Sci. Rep. 7 (2017) 11371, https://doi.org/10.1038/s41598-017-11001-w.
[27] Y. Zhang, J.G. Gigax, T.J. Nizolek, J.S. Carpenter, M.M. Schneider, N. Li, L. Capolungo, R.J. McCabe, Tensile and failure behaviors of Cu/Nb nanolaminates: the effects of loading direction, layer thickness, and annealing, Acta Mater. 240 (2022) 118346, https://doi.org/10.1016/j.actamat.2022.118346.
[28] J. Li, W. Lu, J. Gibson, S. Zhang, T. Chen, S. Korte-Kerzel, D. Raabe, Eliminating deformation incompatibility in composites by gradient nanolayer architectures, Sci. Rep. 8 (2018) 16216, https://doi.org/10.1038/s41598-018-34369-9.
[29] J.J. Li, W.J. Lu, J. Gibson, S.Y. Zhang, S. Korte-Kerzel, D. Raabe, Compatible deformation and extra strengthening by heterogeneous nanolayer composites, Scr. Mater. 179 (2020) 30–35, https://doi.org/10.1016/j.scriptamat.2020.01.006.
[30] J. Li, F. Qin, D. Yan, W. Lu, J. Yao, Shear instability in heterogeneous nanolayered Cu/Zr composites, J. Mater. Sci. Technol. 105 (2022) 81–91, https://doi.org/10.1016/j.jmst.2021.06.070.
[31] F. Qin, W. Lu, J. Li, Enhanced resistance to shear instability by gradient nanolayered structures in sputtered Cu/Zr composites, Mater. Sci. Eng. A 846 (2022) 143253, https://doi.org/10.1016/j.msea.2022.143253.
[32] Y. Wang, J. Li, J. Li, S. Chen, On the strain delocalization mechanism of Cu/Nb nanolayered composites with amorphous interfacial layers, Int. J. Plast. 172 (2024) 103856, https://doi.org/10.1016/j.ijplas.2023.103856.
[33] W. Qiang, Q. Wu, L. Long, Potential regulation of strength-ductility by nucleation and growth mechanisms of shear bands in heterogeneous laminates, Mater. Today Commun. 38 (2024) 107960, https://doi.org/10.1016/j.mtcomm.2023.107960.
[34] G. Wu, C. Liu, L. Sun, Q. Wang, B. Sun, B. Han, J.J. Kai, J. Luan, C.T. Liu, K. Cao, Y. Lu, L. Cheng, J. Lu, Hierarchical nanostructured aluminum alloy with ultrahigh strength and large plasticity, Nat. Commun. 10 (2019) 5099, https://doi.org/10.1038/s41467-019-13087-4.
[35] Y. Chen, N. Li, R.G. Hoagland, X.Y. Liu, J.K. Baldwin, I.J. Beyerlein, J.Y. Cheng, N. A. Mara, Effects of three-dimensional Cu/Nb interfaces on strengthening and shear banding in nanoscale metallic multilayers, Acta Mater. 199 (2020) 593–601, https://doi.org/10.1016/j.actamat.2020.08.019.
[36] Y. Huang, F. Qin, K. Dai, S. Chen, J. Li, J. Li, Substantial toughening by thick nanoscale amorphous intergranular films in nanocrystalline materials, J. Appl. Phys. 134 (2023) 235101, https://doi.org/10.1063/5.0174295.
[37] X. Tao, Y. Lou, M. Li, N. Zhao, X. Tang, H. Hu, X. Huang, J. Yue, Microstructure and mechanical properties of VAlN/Si3N4 nano-multilayer coatings, J. Cent. South Univ. 29 (2022) 1403–1411, https://doi.org/10.1007/s11771-022-5005-x.
[38] H.R. Peng, W.T. Huo, W. Zhang, S. Zhang, Y. Tang, G. Chang, L. Li, X. Li, L.L. Dong, F. Liu, Maximizing the yield stress via synergistic optimization of grain sizes and solute concentrations in extremely fine nanograined metals: a molecular dynamics study, Mater. Today Commun. 38 (2024) 108075, https://doi.org/10.1016/j.mtcomm.2024.108075.
[39] A. Khalajhedayati, Z. Pan, T.J. Rupert, Manipulating the interfacial structure of nanomaterials to achieve a unique combination of strength and ductility, Nat. Commun. 7 (2016) 10802, https://doi.org/10.1038/ncomms10802.
[40] N.Q. Vo, J. Schäfer, R.S. Averback, K. Albe, Y. Ashkenazy, P. Bellon, Reaching theoretical strengths in nanocrystalline Cu by grain boundary doping, Scr. Mater. 65 (2011) 660–663, https://doi.org/10.1016/j.scriptamat.2011.06.048.
[41] H. Van Swygenhoven, P.M. Derlet, A.G. Frøseth, Nucleation and propagation of dislocations in nanocrystalline fcc metals, Acta Mater. 54 (2006) 1975–1983, https://doi.org/10.1016/j.actamat.2005.12.026.
[42] G. Wu, K.C. Chan, L. Zhu, L. Sun, J. Lu, Dual-phase nanostructuring as a route to high-strength magnesium alloys, Nature 545 (2017) 80–83, https://doi.org/10.1038/nature21691.
[43] T. Yang, Y.L. Zhao, W.P. Li, C.Y. Yu, J.H. Luan, D.Y. Lin, L. Fan, Z.B. Jiao, W.H. Liu, X.J. Liu, J.J. Kai, J.C. Huang, C.T. Liu, Ultrahigh-strength and ductile superlattice alloys with nanoscale disordered interfaces, Science 369 (2020) 427–432, https://doi.org/10.1126/science.abb6830.
[44] C.M. Grigorian, T.J. Rupert, Critical cooling rates for amorphous-to-ordered complexion transitions in Cu-rich nanocrystalline alloys, Acta Mater. 206 (2021) 116650, https://doi.org/10.1016/j.actamat.2021.116650.
[45] T.J. Rupert, The role of complexions in metallic nano-grain stability and deformation, Curr. Opin. Solid State Mater. Sci. 20 (2016) 257–267, https://doi.org/10.1016/j.cossms.2016.05.005.
[46] W.F. Yang, M.Y. Gong, J.H. Yao, J.W. Wang, S.J. Zheng, X.L. Ma, Hardening induced by dislocation core spreading at disordered interface in Cu/Nb multilayers, Scr. Mater. 200 (2021) 113917, https://doi.org/10.1016/j.scriptamat.2021.113917.
[47] C.M. Grigorian, T.J. Rupert, Thick amorphous complexion formation and extreme thermal stability in ternary nanocrystalline Cu-Zr-Hf alloys, Acta Mater. 179 (2019) 172–182, https://doi.org/10.1016/j.actamat.2019.08.031.
[48] C.M. Grigorian, T.J. Rupert, Multi-principal element grain boundaries: stabilizing nanocrystalline grains with thick amorphous complexions, J. Mater. Res 37 (2022) 554–566, https://doi.org/10.1557/s43578-021-00459-0.
[49] S. Shao, H.M. Zbib, I.N. Mastorakos, D.F. Bahr, The void nucleation strengths of the Cu–Ni–Nb- based nanoscale metallic multilayers under high strain rate tensile loadings, Comput. Mater. Sci. 82 (2014) 435–441, https://doi.org/10.1016/j.commatsci.2013.09.036.
[50] W. Pang, X. Feng, R. Chen, A. Liu, K. Xin, Molecular dynamics studies of the effect of intermediate Fe layer thickness on the enhanced strength and ductility of Cu/Fe/Ni multilayer, Phys. Scr. 98 (2023) 075942, https://doi.org/10.1088/1402-4896/acdf91.
[51] A. Bellou, C.T. Overman, H.M. Zbib, D.F. Bahr, A. Misra, Strength and strain hardening behavior of Cu-based bilayers and trilayers, Scr. Mater. 64 (2011) 641–644, https://doi.org/10.1016/j.scriptamat.2010.12.009.
[52] J.W. Yan, G.P. Zhang, X.F. Zhu, H.S. Liu, C. Yan, Microstructures and strengthening mechanisms of Cu/Ni/W nanolayered composites, Philos. Mag. 93 (2013) 434–448, https://doi.org/10.1080/14786435.2012.722233.
[53] Y.D. Wang, J.J. Li, Strengthening Cu/Ni nanolayered composites by introducing thin Ag interlayers: a molecular dynamics simulation study, J. Appl. Phys. 130 (2021) 045109, https://doi.org/10.1063/5.0052978.
[54] M.Z. Xiang, Y. Liao, K. Wang, G. Lu, J. Chen, Shock-induced plasticity in semi-coherent {111} Cu-Ni multilayers, Int. J. Plast. 103 (2018) 23–38, https://doi.org/10.1016/j.ijplas.2017.12.005.
[55] Y.D. Wang, J.J. Li, W.J. Lu, F.P. Yuan, X.L. Wu, Enhanced co-deformation of a heterogeneous nanolayered Cu/Ni composite, J. Appl. Phys. 126 (2019) 215111, https://doi.org/10.1063/1.5121625.
[56] Y. Liu, D. Bufford, H. Wang, C. Sun, X. Zhang, Mechanical properties of highly textured Cu/Ni multilayers, Acta Mater. 59 (2011) 1924–1933, https://doi.org/10.1016/j.actamat.2010.11.057.
[57] P. Hirel, Atomsk: a tool for manipulating and converting atomic data files, Comput. Phys. Commun. 197 (2015) 212–219, https://doi.org/10.1016/j.cpc.2015.07.012.
[58] S. Plimpton, Fast parallel algorithms for short-range molecular dynamics, J. Comput. Phys. 117 (1995) 1–19, https://doi.org/10.1006/jcph.1995.1039.
[59] X.W. Zhou, R.A. Johnson, H.N.G. Wadley, Misfit-energy-increasing dislocations in vapor-deposited CoFe/NiFe multilayers, Phys. Rev. B 69 (2004) 144113, https://doi.org/10.1103/PhysRevB.69.144113.
[60] A. Stukowski, Visualization and analysis of atomistic simulation data with OVITO-the open visualization tool, Model Simul. Mater. Sc. 18 (2010) 015012, https://doi.org/10.1088/0965-0393/18/1/015012.
[61] M. Nasim, Y. Li, M. Wen, C. Wen, High-strength Ni/Al nanolaminates fabricated by magnetron sputtering and their nanoindentation and nanowear behaviors, Materialia 6 (2019) 100263, https://doi.org/10.1016/j.mtla.2019.100263.
[62] X. Liu, R. Hao, S. Mao, S.J. Dillon, Shear strengths of FCC-FCC cube-on-cube interfaces, Scr. Mater. 130 (2017) 178–181, https://doi.org/10.1016/j.scriptamat.2016.11.038.
[63] R. Saha, W.D. Nix, Effects of the substrate on the determination of thin film mechanical properties by nanoindentation, Acta Mater. 50 (2002) 23–38, https://doi.org/10.1016/S1359-6454(01)00328-7.
[64] Y.F. Zhang, S. Xue, Q. Li, J. Li, J. Ding, T.J. Niu, R. Su, H. Wang, X. Zhang, Size dependent strengthening in high strength nanotwinned Al/Ti multilayers, Acta Mater. 175 (2019) 466–476, https://doi.org/10.1016/j.actamat.2019.06.028.
[65] J.Y. Zhang, X. Zhang, R.H. Wang, S.Y. Lei, P. Zhang, J.J. Niu, G. Liu, G.J. Zhang, J. Sun, Length-scale-dependent deformation and fracture behavior of Cu/X (X=Nb, Zr) multilayers: The constraining effects of the ductile phase on the brittle phase, Acta Mater. 59 (2011) 7368–7379, https://doi.org/10.1016/j.actamat.2011.08.016.
[66] X.Y. Chen, X.F. Kong, A. Misra, D. Legut, B.N. Yao, T.C. Germann, R.F. Zhang, Effect of dynamic evolution of misfit dislocation pattern on dislocation nucleation and shear sliding at semi-coherent bimetal interfaces, Acta Mater. 143 (2018) 107–120, https://doi.org/10.1016/j.actamat.2017.10.012.
[67] S. Shao, J. Wang, I.J. Beyerlein, A. Misra, Glide dislocation nucleation from dislocation nodes at semi-coherent {1 1 1} Cu–Ni interfaces, Acta Mater. 98 (2015) 206–220, https://doi.org/10.1016/j.actamat.2015.07.044.
[68] A. Selimov, K. Chu, D.L. McDowell, Effects of interdiffusion on shear response of semi-coherent {111} interfaces in Ni/Cu, Int. J. Plast. 157 (2022) 103393, https://doi.org/10.1016/j.ijplas.2022.103393.